chemistry

MDPI

Communication

Chirality Transfer in a Calixarene-Based Directional Pseudorotaxane Complex

Gerardo Concilio [1], Carmine Gaeta [1], Paolo Della Sala [1], Veronica Iuliano [1], Carmen Talotta [1], Guglielmo Monaco [1], Stefano Superchi [2], Sandra Belviso [2] and Placido Neri [1,*]

[1] Dipartimento di Chimica e Biologia "A. Zambelli", Università di Salerno, Via Giovanni Paolo II, I-84084 Fisciano (SALERNO), Italy; conciliogerardo@gmail.com (G.C.); cgaeta@unisa.it (C.G.); pdellasala@unisa.it (P.D.S.); viuliano@unisa.it (V.I.); ctalotta@unisa.it (C.T.); gmonaco@unisa.it (G.M.)

[2] Dipartimento di Scienze, Università della Basilicata, 85100 Potenza, Italy; stefano.superchi@unibas.it (S.S.); sandra.belviso@unibas.it (S.B.)

* Correspondence: neri@unisa.it

Abstract: Hexamethoxycalix[6]arene **3** forms a directional pseudorotaxane complex with the chiral axle (*S*)-(α-methyl-benzyl)benzylammonium **2**$^+$. Between the two (*endo-chiral*)-**2**$^+$**@3** and (*exo-chiral*)-**2**$^+$**@3** pseudorotaxane stereoisomers, the former is preferentially formed. This result confirms the validity of the "*endo*-α-methyl-benzyl rule", previously reported by us. DFT calculations suggest that C-H···π interactions between the methyl group of **2**$^+$ and the calixarene aromatic rings, determine the stereoselectivity of the threading process toward the "*endo-α-methyl-benzyl preference*". An amplification of optical rotation is observed upon formation of the pseudorotaxane complex (*endo-chiral*)-**2**$^+$**@3** with respect to free axle **2**$^+$**.** Thus, the specifical rotation of the 1:1 mixture of chiral **2**$^+$·B(ArF)$_4^-$ salt and achiral **3** was augmented upon formation of the pseudorotaxane and DFT calculations were used to rationalize this result.

Keywords: calixarene; pseudorotaxane; chirality transfer; expanding coefficient

Citation: Concilio, G.; Gaeta, C.; Sala, P.D.; Iuliano, V.; Talotta, C.; Monaco, G.; Superchi, S.; Belviso, S.; Neri, P. Chirality Transfer in A Calixarene-Based Directional Pseudorotaxane Complex. *Chemistry* **2021**, *3*, 1089–1100. https://doi.org/10.3390/chemistry3030079

Academic Editor: Alessandro Ponti

Received: 5 September 2021
Accepted: 15 September 2021
Published: 18 September 2021

1. Introduction

Over the past years, a considerable attention has been devoted to the synthesis of chiral mechanomolecules [1,2] for applications in enantioselective catalysis [3–8], recognition and sensing of chiral analytes [9,10], and the study of chiroptical properties of mechanically interlocked molecules (MIMs) [1,2]. The formation of mechanomolecules [11–14] is generally obtained by pseudorotaxane precursors in which a linear molecule (axle) is threaded through a macrocyclic component (wheel) [15]. Pseudorotaxane complexes are stabilized by means of weak secondary interactions, such as hydrogen bond, halogen bond, π-stacking, cation-π, or metal coordination [11–14]. Starting by pseudorotaxanes, MIMs (such as catenanes and rotaxanes) are generally obtained by convenient synthetic routes such as threading-followed-by-stoppering or macrocyclization strategies [15]. The most common strategy to obtain chiral mechanomolecules is to use components bearing a classical stereogenic element to give a chiral axle and/or a chiral wheel [1,2]. In this case, tedious resolution steps can be avoided by resorting to suitable enantiopure moieties available from the chiral pool [1,2].

Interestingly, when one of the components of a mechanomolecule contains stereogenic elements that display optical rotation and related chiroptical properties, then these properties can be transferred within the whole mechanomolecule and amplified [16–20]. For example, Leigh and co-workers reported a chiral rotaxane in which the chirality was transferred from the axle bearing a stereogenic center, and the mechanomolecule displayed significantly stronger CD (circular dichroism) signals than the free axle [21]. Surprisingly, chiral information can be transferred from a chiral

component to an achiral one of a mechanomolecule, and in this case a chiroptical response can be expected from the achiral part [22,23].

Over the past ten years, our group has shown that the threading of scarcely preorganized calix[6]arene macrocycles (e.g., **3**, Scheme 1) with dialkylammonium axles (e.g., $\mathbf{1}^+$) occurs in $CDCl_3$ when the ammonium linear system is coupled with the weakly coordinating barfate anion tetrakis[3,5-bis(tri-fluoromethyl)phenyl]borate $[B(Ar^F)_4]^-$ (Figure 1) "superweak anion" [24–26]. This method was defined, in short, as the "superweak anion approach" [24–26]. Interestingly, we also observed that the threading of alkylbenzylammonium cations (e.g., $\mathbf{1}^+$) may result in two different stereoisomeric pseudorotaxanes [27], in which the alkyl or the benzyl moiety is hosted inside the calixarene cavity [e.g.: (*endo-alkyl*)-$\mathbf{1}^+$**@3** and (*endo-benzyl*)-$\mathbf{1}^+$**@3**]. These have been termed as "*endo*-alkyl" or "*endo*-benzyl" isomers, respectively (Figure 1). The *endo*-alkyl "orientational mechanostereoisomer" is usually preferred (Figure 1), thus leading to the definition of the so-called "*endo*-alkyl rule" [27]: threading of a directional alkylbenzylammonium axle through a hexaalkoxycalix[6]arene occurs with an endo-alkyl preference.

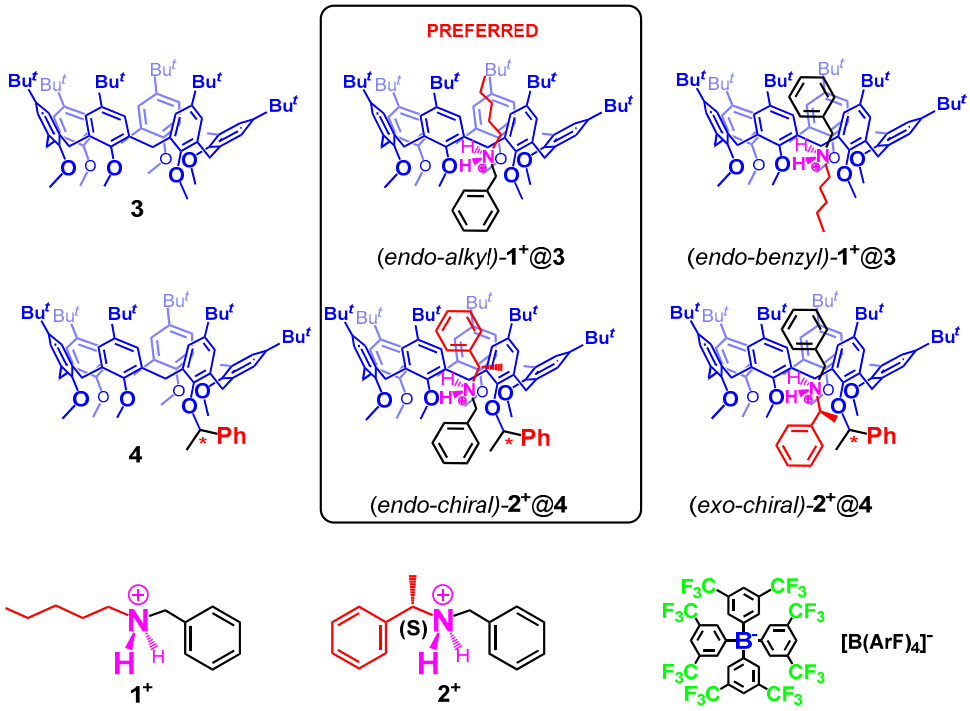

Figure 1. Chemical drawing of calix[6]-wheels **3** and **4**, dialkylammonium ammonium axles $\mathbf{1}^+$ and $\mathbf{2}^+$ used as barfate salts $[B(Ar^F)_4]^-$, and their pseudorotaxane architectures.

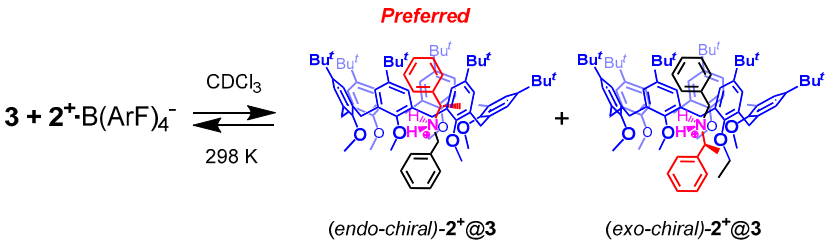

Scheme 1. Threading equilibrium between hexamethoxycalix[6]arene **3** and (*α*-methylbenzyl)benzylammonium axle $\mathbf{2}^+$ as barfate salt. 1D and 2D NMR analysis of the mixture of **3** and $\mathbf{2}^+{\cdot}[B(Ar^F)_4]^-$ indicated the preferential formation of the (*endo-chiral*)-$\mathbf{2}^+$**@3**.

More recently, the formation of calixarene-based chiral pseudorotaxanes (e.g.: (*endo-chiral*)-**2**$^{+}$**@4** in Figure 1) has been investigated by us [28], exploiting cationic axles (e.g.: **2**$^{+}$) and calix[6]-wheels (e.g.: **4**) bearing classical stereogenic centers. In particular, we observed that the threading of chiral calix[6]arene **4** with chiral directional (α-methyl-benzyl)benzylammonium axle **2**$^{+}$ occurs with an *endo*-α-methyl-benzyl preference [28]. In detail, the threading between **4** and **2**$^{+}$ led to the stereoselective formation of (*endo-chiral*)-**2**$^{+}$**@4**.

Considering these results, the question arises as to whether chiral directional (α-methyl-benzyl)benzylammonium axle **2**$^{+}$ can thread the achiral calix[6]arene **3** (Figure 1)**.** Can the chiral axle **2**$^{+}$ transfer chiral properties to achiral calix[6]-wheel **3**? Can some chiroptical properties, such as ORD (optical rotatory dispersion) of axle **2**$^{+}$, be amplified upon its threading inside the achiral calix[6]-wheel **3**?

2. Materials and Methods

2.1. General Details

All the reagents and solvents were purchased from commercial suppliers and used without purifications.

2.2. Synthesis and Characterization of Hexamethoxycalix[6]arene 3 and (α-Methyl-Benzyl)Benzylammonium Axle 2^{+} *as Barfate Salt*

The synthesis of hexamethoxycalix[6]arene **3** [14b] and (*S*)-(α-methyl-benzyl)benzylammonium axle **2**$^{+}$ as barfate salt [28] were performed as previously described in the literature.

2.3. Synthesis and Characterization of the Pseudo[2]Rotaxane (Endo-Chiral)-2^{+}*@3*

1D and 2D NMR experiments. Calixarene derivative **3** (1.9×10^{-3} mmol) was dissolved in 0.5 mL of $CDCl_3$ (3.8×10^{-3} M solution). Then, **2**$^{+}$·$[B(Ar^F)_4]^-$ salt was added (1.9×10^{-3} mmol, 3.8×10^{-3} M) and the mixture was stirred for 15 min. Then, the solution was transferred in an NMR tube for 1D NMR and 2D NMR spectra acquisition. NMR spectra were recorded on Bruker Avance-600 spectrometer [600.13 MHz (^{1}H) and 150.03 MHz (^{13}C)], chemical shifts are reported relative to the residual solvent peak ($CHCl_3$: δ 7.26, $CDCl_3$: δ 77.23).

Optical rotations of pure **2**$^{+}$·$[B(Ar^F)_4]^-$ and of a 1:1 mixture (3.00×10^{-3} M) of **3** and **2**$^{+}$·$[B(Ar^F)_4]^-$ salt were measured at room temperature in $CHCl_3$ on a JASCO DIP-370 digital polarimeter using a 1.0 dm cell. Measurements at different wavelengths were carried out employing a Na lamp for measurement at 589 nm and a Hg lamp with appropriate filters for measurements at 546 nm, 435 nm, and 405 nm, respectively. $[\alpha]_\lambda$ values are given in deg·cm^3·g^{-1}·dm^{-1} and concentration *c* is expressed in g/100 mL.

2.4. Computational Details

All the screening procedures for the search of the most stable conformers were made employing the Amber ff99SB [29] force field as implemented in YASARA [30]. DFT calculations were performed with the Gaussian16 suite of programs [31]. All stationary points were characterized by all real frequencies. Thermodynamic corrections were calculated at 298.15 K and 1 atm for the optimized geometries. Natural Bond Orbital (NBO) analyses were obtained with NBO 3.1 version implemented in Gaussian 16. ORD was calculated on the optimized geometries by the CPHF approach at the B3LYP/6-31G(2d,1p) level coupled with the PCM to describe the effect of chloroform. The molecular surfaces of the guest inside the cavity (SGuest) were computed by YASARA software, which also permits the direct measure of the contact surface between guest and host (SContact). The values of $V_{complexed\_Host}$ and V_{free_Host} were measured with the Caver analyst software employing 1,000,000 of number of samples [32]. In all the cases a probe of 1.0 Å was used.

3. Results

Following a protocol previously reported by us [24–26] and others [33], we have preliminarily studied the threading of **3** with $\mathbf{2}^+$ by 1D and 2D NMR experiments (Scheme 1 and Figure 2). The ^{1}H NMR spectrum of a 1:1 mixture of **3** and $\mathbf{2}^+\cdot[B(Ar^F)_4]^-$ salt in $CDCl_3$ at 25 °C (Figure 2a,b) showed, immediately after mixing, substantial changes that indicated the formation of pseudorotaxane $\mathbf{2}^+$**@3** (Scheme 1, Figure 2d) by a threading equilibrium slow on the NMR timescale.

Diagnostic shielded aromatic signals attributable to the benzylic unit (*ortho*-BnH (*o*), *meta*-BnH (*m*), and *para*-BnH (*p*), see Figure 2) hosted inside the calixarene cavity, were detected, respectively, at 4.58, 5.64, and 6.22 ppm [24–26].

At this point, we studied the stereoselectivity of the threading of **3** with axle $\mathbf{2}^+$. As indicated in Scheme 1, two possible stereoisomeric pseudo[2]rotaxanes are here expected; namely, (*endo-chiral*)-$\mathbf{2}^+$**@3** and (*exo-chiral*)-$\mathbf{2}^+$**@3**, in which the stereogenic center is placed inside or outside the calix-cavity, respectively.

Previously [28] we showed that in the presence of chiral calix[6]arene derivative **4** (Figure 1) the chiral (α-methyl-benzyl)benzylammonium axle $\mathbf{2}^+$ forms the (*endo-chiral*)-$\mathbf{2}^+$**@4** pseudorotaxane diastereoisomer (Figure 1) in which the calix-cavity prefers to host the α-methyl-benzyl group with respect to the simple unsubstituted benzyl group as in (*exo-chiral*)-$\mathbf{2}^+$**@4**. DFT calculations suggested that, in addition to the fundamental H-bonding N-H···O^{Calix} interactions, the α-methyl group establishes additional stabilizing secondary C–H···π interactions with the aromatic walls which favor the preferential formation of the "endo-chiral" diastereoisomer. Based on these results, we introduced [28] a new stereoselectivity rule (named "*endo*-α-methyl-benzyl rule") for the threading of calixarene macrocycles: "*threading of a hexaalkoxycalix[6]arene with a directional (α-methyl-benzyl)benzylammonium axle occurs with an* endo-*α-methyl-benzyl preference*". Based on these considerations, the question arises if the "*endo*-α-methyl-benzyl rule" is still valid using achiral hexamethoxycalix[6]arene wheel **3**. The negative region of the ^{1}H NMR spectrum of pseudorotaxane $\mathbf{2}^+$**@3** (Figure 2a,b) showed the presence of a diagnostic doublet at −0.93 ppm (labeled "a" in Figure 2) attributable to the methyl group of the α-methylbenzyl moiety shielded by the aromatic walls. Interestingly, the benzylic-CH hydrogen atom ("b" in Figure 2) was detected at 1.73 ppm by a 2D COSY correlation (Figure 2c,d). This result confirms that the "*endo*-α-methyl-benzyl rule" is valid also when (*S*)-(α-methyl-benzyl)benzylammonium axle $\mathbf{2}^+$ is threaded in achiral calix[6]arene **3**, and consequently (*endo-chiral*)-$\mathbf{2}^+$**@3** is the preferred pseudorotaxane stereoisomer. An apparent association constant of K_{app} = 148 ± 20 M^{-1} for (*endo-chiral*)-$\mathbf{2}^+$**@3** complex was determined by integration of ^{1}H NMR signals [34] of the 1:1 titration mixture in $CDCl_3$ (Figure 2b), which showed slowly exchanging signals for both free and complexed host (marked in red and magenta in Figure 2b, respectively). DFT calculations at the B3LYP/6-31G(d,p) level of theory [31] were performed on pseudorotaxane (*endo-chiral*)-$\mathbf{2}^+$**@3** (Figure 3). A close inspection of the optimized pseudo[2]rotaxane structure (Figure 3a) reveals the presence of typical H-bonds between the ammonium group of $\mathbf{2}^+$ axle and the oxygen atom at the lower rim of the calix[6]arene-wheel (N···O average distance of 3.0 Å and N-H···O angle of 156.6°). Stabilizing C-H···π interactions [35] between the H-atoms of the methyl group of $\mathbf{2}^+$ and the calixarene aromatic walls (C-H···$\pi^{centroid}$ distance of 2.6 Å and C-H···$\pi^{centroid}$ angle of 143.3°) [35] play a crucial role in directing the stereoselectivity of the threading process toward the "endo-*α-methyl-benzyl preference*". This result agrees with the lower theoretical energy of (*endo-chiral*)-$\mathbf{2}^+$**@3**pseudorotaxane by 1.5 kcal/mol with respect to the *exo-chiral* isomer.

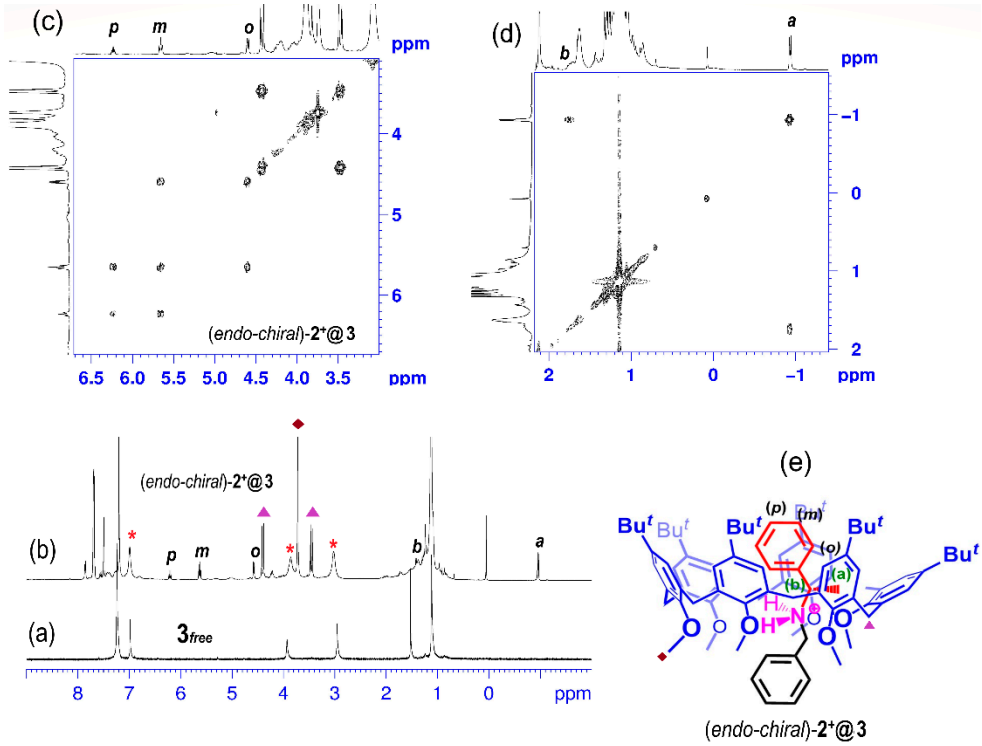

Figure 2. ^{1}H NMR spectra (600 MHz, 298 K, $CDCl_3$) of: (**a**) hexamethoxycalix[6]arene **3**; (**b**) (*endo-chiral*)-**2**$^+$**@3** pseudorotaxane; (**c**,**d**) Significant expansions of 2D COSY spectrum of (*endo-chiral*)-**2**$^+$**@3** pseudorotaxane; (**e**) Chemical drawing of (*endo-chiral*)-**2**$^+$**@3** pseudorotaxane.

To further investigate the energy contribution due to non-covalent interactions (NCI) [36], an SOPT analysis [37] of the Fock matrix in the NBO basis was carried out. Interestingly, the SOPT analysis conducted on (*endo-chiral*)-**2**$^+$**@3** pseudo[2]rotaxane (Table S2) indicated the presence of a network of hydrogen bonding interactions, in addition to C-H···π and π···π interactions. In particular, we evidenced two LP(2)→σ* donations between an oxygen atom of **3** and a N-H antibonding orbital of **2**$^+$ (Table S2). These interactions give an energetic contribution of 6.10 and 9.23 kcal/mol, respectively, for a total energy of 15.33 kcal/mol (Table S2), that accounts for 46% of the overall energy due to secondary non-covalent interactions (NCI, 28.47 kcal/mol). Interestingly, an interaction was detected between aromatic ring of **3** with a C–H antibonding orbital of **2**$^+$ that gives a contribution of 0.93 kcal/mol. Stabilizing C-H···π interactions were detected between the methyl group of axle **2**$^+$ hosted inside the calix-cavity and the aromatic group of **3** by means of a donation between the aromatic ring of **3** and a CH_2-H antibonding orbital of **2**$^+$, that accounted for 1.59 kcal/mol.

Very recently, our group proposed the *Expanding Coefficient* (EC in equation 1) [38], as a new parameter, that can be correlated with the thermodynamic stability of supramolecular complexes governed by weak secondary interactions and obeying the induced-fit model. EC is considered as a single-value geometrical parameter, which considers the energy cost associated with the host reorganization upon induced-fit complexation.

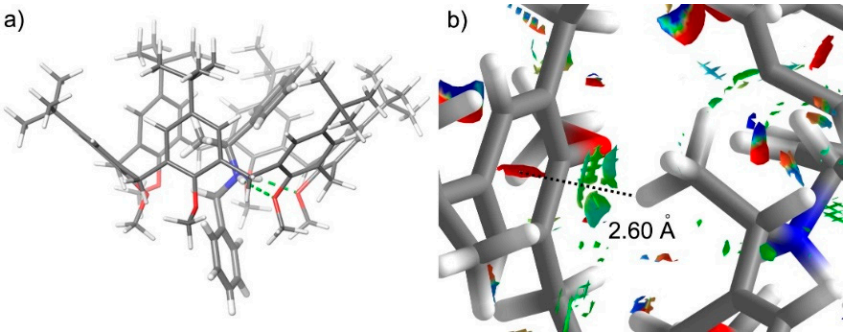

Figure 3. (**a**) DFT-optimized structures of the (*endo-chiral*)-**2**$^{+}$**@3** complex at the B3LYP/6- 31G(d,p) level of theory. Dashed lines represent H-bonding interactions between ammonium group of **2**$^{+}$ and oxygen atoms of **3**. (**b**) NCI plot by the sign of the second Hessian eigenvalue [gradient isosurfaces (s = 0.6 a.u.) for (*endo-chiral*)-**2**$^{+}$**@3** complex. In the coloring isosurface, blue and green colors represent strong and medium interactions (H-bonding and van der Waals). Highlighted the CH_2–H···π distance between the methyl group of axle **2**$^{+}$ and an anisole ring of the calix[6]-wheel.

Expanding Coefficient (EC, equation 1) is defined as the ratio between the final and the initial cavity volumes of the host, i.e., the volume of the host cavity after the complexation ($V_{\text{complexed\_host}}$ at the global minimum) and that of the host cavity before the complexation ($V_{\text{free\_host}}$ at the global minimum) [38].

$$\text{EC} = \frac{V_{\text{complexed\_host}}}{V_{\text{free\_host}}} \quad (1)$$

The values of $V_{\text{complexed\_host}}$ and $V_{\text{free\_host}}$ were measured by using the DFT-optimized structures of the separated host and guest for the (*endo-chiral*)-**2**$^{+}$**@3** and (*exo-chiral*)-**2**$^{+}$**@3** complexes (see the Supplementary Materials) with the Caver software [32].

Previously, we showed [38] that EC values of dialkylammonium@calix[6]arene complexes had a good linear correlation with the thermodynamic stabilities of the complexes (see Figure 4a, points in blue light). In other words, a higher EC value implies a higher deformation of the host, which in turn implies a higher energetical cost. Consequently, low EC values were correlated with high thermodynamic stabilities. In fact, the analysis of EC values reported recently for dialkylammonium@calix[6]arene complexes, which were stabilized by weak intermolecular interactions (dispersion forces, van der Waals interactions), showed that the primary determinant to the stability of induced-fit complexes was the degree of deformation of the host with respect to the ground conformation.

Based on these considerations, we decided to verify if the thermodynamic stability of (*endo-chiral*)-**2**$^{+}$**@3** and (*exo-chiral*)-**2**$^{+}$**@3** complexes are also correlating with the EC parameter.

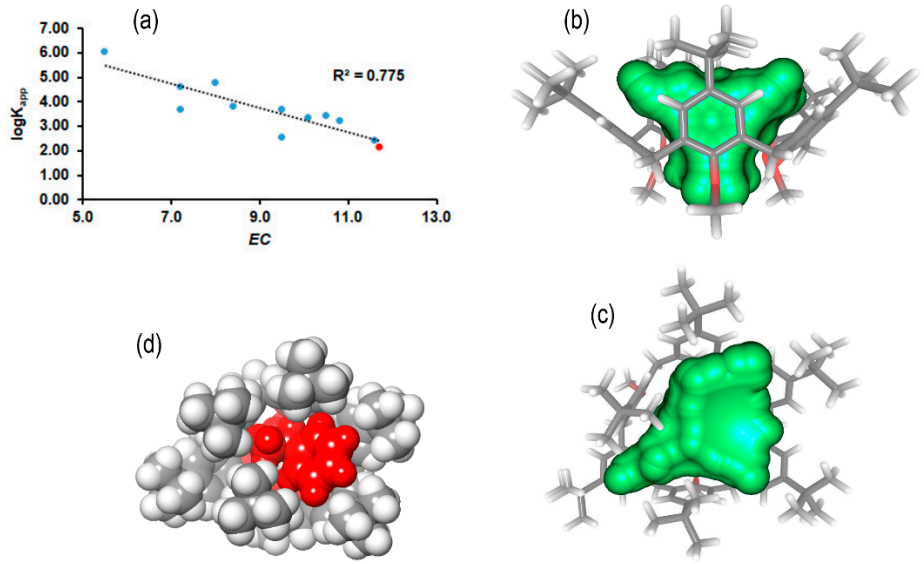

Figure 4. (**a**) Linear regression analysis of log K_{app} vs EC for alkylbenzylammonium-based pseudorotaxane complexes: points colored in light blue represent log K_{app}/EC values reported in reference [38], while in red is indicated the log K_{app}/EC value of the (*endo-chiral*)-**2**$^{+}$**@3** complex. (**b**,**c**) Different views of the final cavity volumes of **3** in cone conformation, upon *endo-chiral* complexation with **2**$^{+}$ The initial volume of the free host **3** has been calculated considering the calix[6]arene in 1,2,3-alternate conformation, in accord with the protocol reported previously by us [38]. (**d**) Top view of the DFT-optimized structure of (*endo-chiral*)-**2**$^{+}$**@3** complex, in red (*S*)-(*α*-methylbenzyl)benzylammonium axle **2**$^{+}$ guest.

Close inspection of Figure 4 clearly reveals that upon formation of the (*endo-chiral*)-**2**$^{+}$**@3** complex, the calix[6]arene-wheel adopts a deformed cone-1,4-out conformation, approaching an asymmetrical cone-1,2,4-out geometry (also see Figure 4), and it is evident that, during the induced-fit recognition process, the calix-cavity deforms, allowing the change of the void volume of the receptor. Close inspection of Figure 4 indicates a substantial change of void volume between complexed host (Figure 4b) and free host in 1,2,3-alternate conformation [38] (Figure 4a). In detail, an EC value of 11.7 was calculated for the complex (*endo-chiral*)-**2**$^{+}$**@3**, which has a good correlation with the low value of K_{app} = 148 ± 20 M^{-1} [38] (Figure S5). A similar calculation provided an EC value of 11.5 for (*exo-chiral*)-**2**$^{+}$**@3** complex, but this value cannot be directly correlated with the previous ones because that dataset was constructed [38] by using the simple unsubstituted benzyl ($PhCH_2$-) as the common *exo*-group for all the complexes. Therefore, the presence of a methyl in the $PhCH(CH)_3$- *exo*-group of (*exo-chiral*)-**2**$^{+}$**@3** complex produces an apparent no-correlating EC value for it.

With these results in hand, now the question arises as to whether the threading of the chiral axle **2**$^{+}$ as barfate salt into the achiral calixarene **3** could induce the stabilization of a chiral conformation of the latter in the pseudo[2]rotaxane (*endo-chiral*)-**2**$^{+}$**@3** and if the presence of such chiral conformation could be detected by optical rotation measurements. In fact, optical rotation has proved to be a very sensitive technique to reveal the induction of chiral conformations in achiral polyaromatic probes through interaction with chiral substrates [39]. If so, we should expect a change of the optical rotation of **2**$^{+}$ upon threading inside the cavity of **3** because the threading process of the chiral ammonium axle **2**$^{+}$ with achiral calix[6]-wheel **3** would generate a pseudo[2]rotaxane with different optical rotations with respect to free chiral component **2**$^{+}$.

To explore this aspect, we performed measurements of specific optical rotation [α] at different wavelengths of the pure chiral **2**$^{+}$·$[B(Ar^F)_4]^-$ salt and of an equimolar mixture (3.00×10^{-3} M) of **3** and **2**$^{+}$ salt in chloroform (Table 1 and Figure 5a). Starting by the initial concentration of **3** and **2**$^{+}$·$[B(Ar^F)_4]^-$ salt (3.00×10^{-3} M) and known the apparent association

constant (K_{ass} = 148 ± 20 M^{-1}) for the equilibrium of formation of the (*endo-chiral*)-**2**$^{+}$**@3** pseudorotaxane in Scheme 1, $[\alpha]_\lambda$ at the equilibrium for the (*endo-chiral*)-**2**$^{+}$**@3** pseudorotaxane has been calculated (Table 1) according to the procedure reported in Supplementary Materials.

The $[\alpha]_\lambda$ values of the (*endo-chiral*)-**2**$^{+}$**@3** pseudorotaxane so calculated have been compared with those measured for the pure chiral axle **2**$^{+}$·$[B(Ar^F)_4]^-$, Table 1.

Table 1. Optical rotations of (*endo-chiral*)-**2**$^{+}$**@3** pseudo[2]rotaxane.[a]

λ(nm)	$[\alpha]_{2+}$[b]	α_{mix}[c]	α_{2+}	$\alpha_{2+@3}$	$[\alpha]_{2+@3}$[d]
589	0.8	−0.030	0.0154	−0.0316	−12.4
546	−4.8	−0.0686	−0.0922	−0.0594	−23.2
435	−14.3	−0.153	−0.2746	−0.1255	−49.0
405	−19.6	−0.195	−0.3763	−0.1572	−61.4

[a] Measured in $CHCl_3$. [b] Specific optical rotation of the pure chiral **2**$^{+}$·$B(ArF)_4^-$ salt *c* = 0.356 g/100mL. [c] Optical rotation of the 1:1 mixture (3.00×10^{-3} M) of **3** and **2**$^{+}$·$[B(Ar^F)_4]^-$ salt. [d] Specific optical rotation of the pure (*endo-chiral*)-**2**$^{+}$**@3** pseudorotaxane (see Supplementary Materials for the procedure).

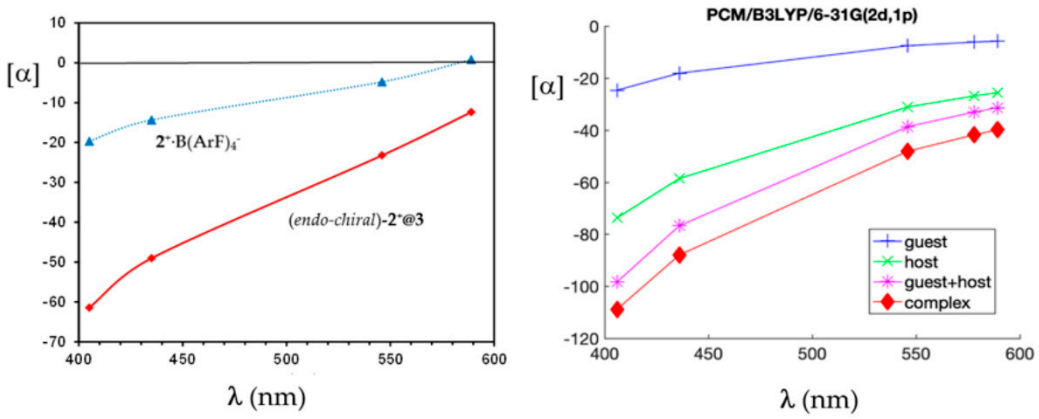

(**a**) (**b**)

Figure 5. (**a**) Specific optical rotation ($[\alpha]$) of the chiral guest **2**$^{+}$·$[B(Ar^F)_4]^-$ salt (blue triangles and dotted blue line) and of the (*endo-chiral*)-**2**$^{+}$**@3** pseudorotaxane (red squares and solid red line) at different wavelength. (**b**) Computed ORD curves calculated at the PCM/B3LYP/6-31G(2d,1p) level of theory, for the (*endo-chiral*)-**2**$^{+}$**@3** complex; isolated guest **2**$^{+}$ (-+-) and host **3** (-x-) blocked in the conformation they have in the complex and the sum of the curves of the isolated guest and host (-*-).

Inspection of the Figure 5 revealed that the optical rotation of **2**$^{+}$·$[B(Ar^F)_4]^-$ salt was amplified upon threading with **3**. In fact, the specifical rotation of the 1:1 mixture of chiral **2**$^{+}$·$[B(Ar^F)_4]^-$ salt and achiral **3** was augmented upon threading. To rationalize these results (Figure 5a), we have computed (Figure 5b) the specific optical rotation in degrees on the complex and on the isolated guest and host at the same geometry of the complex. The availability of the ORD data is most beneficial in cases as this, where at the sodium wavelength optical rotation is too low to be accurately computed with a reasonable computational effort [40]. As can be seen, the complex has a computed ORD which compares favorably with the experiment, although its magnitude is overestimated.

The computed specific rotation of the complex turns out to be close to the sum of the specific rotation of isolated host and guest computed with the same geometry they have in the complex (Figure 5b). This indicates that the main mechanism of amplification of optical rotation comes from the ability of the axle to induce a chiral conformation of the host. The mechanism of amplification of chirality through the interaction of occupied and

virtual orbitals of different units (host and guest) accounts in this case only for a small fraction of the effect (quantifiable from the distance of the red-diamonds and magenta-asterisks curves in Figure 5b as compared to the distance of the red-diamonds from the zero line.). In fact, an inspection of Figure 6a confirms that the host **3** conformation in the complex is asymmetrical due to a higher inclination of one aromatic ring (B in Figure 6a) with respect to the related one (A in Figure 6a). In details, the aromatic rings A and B of **3** in the complex have very different canting angle values of 75.3° and 50.5°, respectively (Table 2). Analogously, the $ArCH_2Ar$ dihedral angles χ_a and ϕ_b (Figure 6a) on opposite positions and adjacent to the A and B aromatic rings of **3** assume very different values (as well as ϕ_a and χ_b, see Table 2). In this way, a perfectly symmetrical cone-1,4-out conformation for calix[6]arene macrocycle is deformed toward an asymmetrical cone-1,2,4-out conformation (Figure 6a), which is therefore responsible of the additional contribution to the optical rotation.

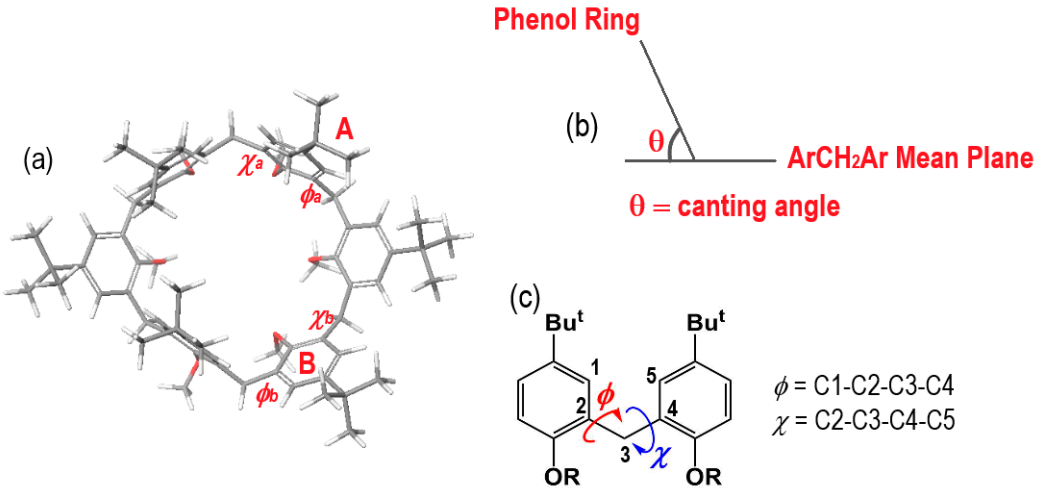

Figure 6. (**a**) Top view of the asymmetrical cone-1,2,4-out conformation of the host **3** in the (*endo-chiral*)-**2**$^+$**@3** complex as obtained by DFT calculations (see Figure 4d). A and B capital letters in (**a**) indicate the aromatic rings of the DFT-optimized structure of **3** in the (*endo-chiral*)-**2**$^+$**@3** complex, considered for the measurements of the canting angles θ, as defined in **b**) (see Table 2). (**c**) $ArCH_2Ar$ ϕ and χ dihedral angles.

Table 2. ϕ And χ $ArCH_2Ar$ dihedral angles adjacent to the aromatic rings A and B (see Figure 6) of **3** and canting angles values of the A and B rings of **3**.[a]

ϕ and χ	Values (°)	Canting	Angles (θ)
χ_a	−78.72	A	75.35°
ϕ_b	106.08		
ϕ_a	50.94	B	50.51°
χ_b	−73.04		

[a] The measurements were performed on the DFT-optimized structure of the (*endo-chiral*)-**2**$^+$**@3** by removing the guest **2**$^+$.

4. Conclusions

In this report we showed that hexamethoxycalix[6]arene **3** can form pseudorotaxane complex with the chiral axle (*S*)-(α-methyl-benzyl)benzylammonium **2**$^+$. The threading is directional: between the two (*endo-chiral*)-**2**$^+$**@3** and (*exo-chiral*)-**2**$^+$**@3**, the former is preferentially formed. This result confirms the validity of the "*endo*-α-methyl-benzyl rule", previously reported by us [28] for the threading of calixarene macrocycles: "*threading of a hexaalkoxycalix[6]arene with a directional (α-methyl-benzyl)benzylammonium axle occurs with an endo-α-methyl-benzyl preference*". DFT calculations suggest that, also in

this case (see reference [28]), stabilizing C-H···π interactions between the methyl group of $\mathbf{2}^+$ and the calixarene benzene rings determine the stereoselectivity of the threading process toward the "endo-*α-methyl-benzyl preference*".

Upon threading inside the cavity of calix-wheel **3** the optical rotation of $\mathbf{2}^+$ is changed; in other words, the threading process of the chiral ammonium axle $\mathbf{2}^+$ with achiral calix[6]-wheel **3** generates a pseudo[2]rotaxane with higher optical rotation with respect to free chiral axle $\mathbf{2}^+$. In detail, the optical rotation of $\mathbf{2}^+\cdot[B(Ar^F)_4]^-$ salt is amplified upon threading with **3**. DFT calculations show that the specific rotation of the complex is close to the sum of the specific rotation of host and guest computed with the same geometry that they have in the complex. This result suggests that the mechanism of amplification of optical rotation comes in our case from a chirality transfer from the axle to the wheel mainly by inducing a chiral conformation of the host, as also recently found for the VCD of a complex of a chiral ammonium salt with an achiral crown ether [10e].

Supplementary Materials: The following are available online, electronic supplementary Material available: 1D and 2D NMR spectra of compounds and (*endo-chiral*)-$\mathbf{2}^+$**@3** pseudorotaxane, the optimized molecular structures for (*endo-chiral*)-$\mathbf{2}^+$**@3** pseudorotaxane, EC calculations, NBO and NCI details, procedure for the calculation of $[\alpha]_\lambda$ at the equilibrium for the (*endo-chiral*)-$\mathbf{2}^+$**@3**. Figure S1: ^{1}H NMR of pseudo[2]rotaxane $\mathbf{2}^+$**@3** ($CDCl_3$, 600 MHz, 298 K); Figure S2: ^{13}C NMR of pseudo[2]rotaxane $\mathbf{2}^+$**@3** ($CDCl_3$, 100 MHz, 298 K); Figure S3: 2D COSY of pseudo[2]rotaxane $\mathbf{2}^+$**@3** ($CDCl_3$, 400 MHz, 298 K); Figure S4: 2D HSQC of pseudo[2]rotaxane $\mathbf{2}^+$**@3** ($CDCl_3$, 600 MHz, 298 K); Figure S5: ^{1}H NMR spectrum of equimolar solution ($3.9\cdot10^{-3}$ M) of **3** and $\mathbf{2}^+\cdot TFPB^-$. The association constant K_{ass} value was calculated by integration of complexed (▲) and free derivative **3** (●) ($CDCl_3$, 400 MHz, 298 K); Figure S6: Minimized structure of (*endo-chiral*)-$\mathbf{2}^+$**@3** (a) lateral and (b) top views. H-Bonds are highlighted with dashed green lines; Figure S7: Minimized structure of (*exo-chiral*)-$\mathbf{2}^+$**@3** (a) lateral and (b) top views. H-Bonds are highlighted with dashed green lines; Figure S8: Linear regression analysis of ECs vs log K_{app} values for pseudo[2]rotaxane based on derivative **3**; Table S1: Second orbital interaction for (*endo-chiral*)-$\mathbf{2}^+$**@3**.

Author Contributions: G.C.: synthesis; P.D.S.: NBO and NCI calculations; V.I.: EC calculations; C.T.: 1D and 2D NMR studies and supervision; G.M.: computation of ORD curves; S.S.: calculation of $[\alpha]_\lambda$ at the equilibrium for the (*endo-chiral*)-$\mathbf{2}^+$**@3;** S.B.: ORD measurements; C.G.: data analysis and manuscript writing; P.N.: data analysis, and conceptualization. All authors have read and agreed to the published version of the manuscript.

Funding: The authors acknowledge the Regione Campania (POR CAMPANIA FESR 2007/2013 O.O.2.1, CUP B46D14002660009) for the FT-ICR mass spectrometer facilities, the "Centro di Tecnologie Integrate per la Salute" (CITIS) (project PONa3_00138) for the 600 MHz NMR facilities. Financial support is acknowledged from the University of Salerno (FARB).

Institutional Review Board Statement: Not applicable.

Informed Consent Statement: Not applicable.

Data Availability Statement: Not applicable.

Conflicts of Interest: The authors declare no conflict of interest.

References

1. Jamieson, E.M.G.; Modicom, F.; Goldup, S.M. Chirality in rotaxanes and catenanes. *Chem. Soc. Rev.* **2018**, *47*, 5266–5311, doi:10.1039/C8CS00097B.
2. Evans, N.H. Chiral Catenanes and Rotaxanes: Fundamentals and Emerging Applications. *Chem. Eur. J.* **2018**, *24*, 3101–3112, doi:10.1002/chem.201704149.
3. Hoekman, S.; Kitching, M.O.; Leigh, D.A.; Papmeyer, M.; Roke, D.; Goldberg Active Template Synthesis of a [2]Rotaxane Ligand for Asymmetric Transition-Metal Catalysis. *J. Am. Chem. Soc.* **2015**, *137*, 7656–7659, doi:10.1021/jacs.5b04726.
4. Heard, A.W.; Goldup, S.M. Synthesis of a Mechanically Planar Chiral Rotaxane Ligand for Enantioselective Catalysis. *Chem.* **2020**, *6*, 994–1006, doi:10.1016/j.chempr.2020.02.006.
5. Cakmak, Y.; Erbas-Cakmak, S.; Leigh, D.A. Asymmetric Catalysis with a Mechanically Point-Chiral Rotaxane. *J. Am. Chem. Soc.* **2016**, *138*, 1749–1751, doi:10.1021/jacs.6b00303.
6. Mitra, R.; Zhu, H.; Grimme, S.; Niemeyer, J. Functional Mechanically Interlocked Molecules: Asymmetric Organocatalysis with a Catenated Bifunctional Brønsted Acid. *Angew. Chem. Int. Ed.* **2017**, *56*, 11456–11459, doi:10.1002/anie.201704647.

7. Tachibana, Y.; Kihara, N.; Takata, T. Asymmetric benzoin condensation catalyzed by chiral rotaxanes tethering a thiazolium salt moiety via the cooperation of the component: Can rotaxane be an effective reaction field? *J. Am. Chem. Soc*. **2004**, *126*, 3438–3439, doi:10.1021/ja039461l.
8. Blanco, V.; Leigh, D.A.; Marcos, V.; Morales-Serna, J.A.; Nussbaumer, A.L. A Switchable [2]Rotaxane Asymmetric Organocatalyst That Utilizes an Acyclic Chiral Secondary Amine. *J. Am. Chem. Soc.* **2014**, *136*, 4905–4908, doi:10.1021/ja501561c.
9. Mitra, R.; Thiele, M.; Octa-Smolin, F.M.; Letzel, C.; Niemeyer, J. A bifunctional chiral [2]catenane based on 1,1′-binaphthyl-phosphates. *Chem. Commun*. **2016**, *52*, 5977–5980, doi:10.1039/C6CC01980C.
10. Lim, J.Y.C.; Marques, I.; Félix, V.; Beer, P.D. Enantioselective Anion Recognition by Chiral Halogen-Bonding [2]Rotaxanes. *J. Am. Chem. Soc*. **2017**, *139*, 12228–12239, doi:10.1021/jacs.7b06144.
11. Bruns, C.J.; Stoddart, J.F. *The Nature of the Mechanical Bond.: From Molecules to Machines, First Edition.* John Wiley & Sons: Hoboken, New Jersey, NJ, USA, **2017**, doi:10.1002/anie.201611682.
12. Feringa, B.L. The art of building small: From molecular switches to motors. *Angew. Chem. Int. Ed.* **2017**, *56*, 11060–11078, doi:10.1002/anie.201702979.
13. Sauvage, J.-P. From chemical topology to molecular machines. *Angew. Chem. Int. Ed.* **2017**, *56*, 11080–11093, doi:10.1002/anie.201702992.
14. Stoddart, J.F. Mechanically interlocked molecules (MIMs)—molecular shuttles, switches, and machines. *Angew. Chem. Int. Ed.* **2017**, *56*, 11094–11125, doi:10.1002/anie.201703216.
15. Sauvage, J.P.; Dietrich-Buchecker, C. Molecular catenanes, rotaxanes and knots: A journey through the world of molecular topology; Wiley-VCH: Weinheim, Germany, 1999.
16. Xing, P.; Zhao, Y. Controlling supramolecular chirality in multicomponent self-assembled systems. *Acc. Chem. Res*. **2018**, *51*, 2324–2334, doi:10.1021/acs.accounts.8b00312.
17. Kuwahara, S.; Chamura, R.; Tsuchiya, S.; Ikeda, M.; Habata, Y. Chirality transcription and amplification by [2]pseudorotaxanes. *Chem. Commun*. **2013**, *49*, 2186–2188, doi:10.1039/c2cc38758a.
18. Wang, H.-J.; Zhang, H.-Y.; Zhang, H.-Y.; Liu, G.; Dai, X.; Wua, H.; Liu, Y. Guest-induced supramolecular chirality transfer in [2]pseudorotaxanes: Experimental and computational study. *Org. Biomol. Chem*. **2020**, *18*, 7649–7655, doi:10.1039/d0ob01347a.
19. Cao, H.; de Feyter, S. Amplification of chirality in surface-confined supramolecular bilayers. *Nat. Commun*. **2018**, *9*, 3416–3425, doi:10.1038/s41467-018-05962-3.
20. Weiricha, L.; Merten, C. Induced VCD and conformational chirality in host–guest complexes of a chiral ammonium salt with crown ethers. *Phys. Chem. Chem. Phys*. **2021**, *23*, 18300–18307, doi:10.1039/D1CP01846A.
21. Asakawa, M.; Brancato, G.; Fanti, M.; Leigh, D.A.; Shimizu, T.; Slawin, A.M.Z.; Wong, J.K.Y.; Zerbetto, F.; Zhang, S. Switching "on" and "off" the expression of chirality in peptide rotaxanes. *J. Am. Chem. Soc*. **2002**, *124*, 2939–2950, doi:10.1021/ja015995f.
22. Saito, S.; Hirano, Y.; Mutoh, Y.; Kasama, T. Synthesis of a Homochiral [2]Rotaxane from a BINOL-derived Macrocyclic Phenanthroline. *Chem. Lett*. **2015**, *44*, 1509–1511, doi:10.1246/cl.150693.
23. Zhu, X.Z.; Chen, C.F. Efficient synthesis of a chiral [4]pseudocatenane and its derivatives: A novel ship's wheel-like interlocked structure. *Chem. Eur. J.* **2006**, *12*, 5603–5609; doi:10.1002/chem.200600195.
24. Gaeta, C.; Talotta, C.; Neri, P. Pseudorotaxane orientational stereoisomerism driven by π-electron density. *Chem. Comm.* **2014**, *50*, 9917–9920, doi: 10.1039/c4cc04668d.
25. Gaeta, C.; Talotta, C.; Farina, F.; Camalli, M.; Campi, G.; Neri, P. Conformational features and recognition properties of a conformationally blocked calix[7]arene derivative. *Chem. Eur. J.* **2012**, *18*, 1219–1230, doi:10.1002/chem.201102179.
26. Della Sala, P.; Talotta, C.; Capobianco, A.; Soriente, A.; de Rosa, M.; Neri, P.; Gaeta, C. Synthesis, optoelectronic, and supramolecular properties of a calix[4]arene–cycloparaphenylene hybrid host. *Org. Lett.* **2018**, *20*, 7415–7418, doi:10.1021/acs.orglett.8b03134.
27. Talotta, C.; Gaeta, C.; Qi, Z.; Schalley, C.A.; Neri, P. Pseudorotaxanes with Self-Sorted Sequence and Stereochemical Orientation. *Angew. Chem. Int. Ed.* **2013**, *52*, 7437–7441, doi:10.1002/anie.201301570.
28. Talotta, C.; Concilio, G.; Della Sala, P.; Gaeta, C.; Schalley, C.A.; Neri, P. Study on the influence of chirality in the threading of calix[6]arene hosts with dialkylammonium axles. *Molecules* **2020**, *25*, 5323–5344, doi:10.3390/molecules25225323.
29. Maier, J.; Martinez, C.; Kasavajhala, K.; Wickstrom, L.; Hauser, K.; Simmerling, C. Improving the accuracy of protein side chain and backbone parameters from ff99SB. *J. Chem. Theory Comput*. **2005**, *11*, 3696–3713, doi:10.1021/acs.jctc.5b00255.
30. Krieger, E.; Vriend, G. YASARA view—molecular graphics for all devices—from smartphones to workstations. *Bioinform*. **2014**, *30*, 2981–2982, doi:10.1093/bioinformatics/btu426. Krieger E.; Vriend, G., New ways to boost molecular dynamics simulations. *J. Comput. Chem.* **2015**, *36*, 996–1007 doi: 10.1002/jcc.23899.
31. Frisch, M.J.; Trucks, G.W.; Schlegel, H.B.; Scuseria, G.E.; Robb, M.A.; Cheeseman, J.R.; Scalmani, G.; Barone, V.; Petersson, G.A.; Nakatsuji, H.; et al. Gaussian 16 Revision C.03; Inc., Wallingford CT, 2016.
32. Jurcik, A.; Bednar, D.; Byska, J.; Marques, S.M.; Furmanova, K.; Daniel, L.; Kokkonen, P.; Brezovsky, J.; Strnad, O.; Stourac, J.; et al. CAVER analyst 2.0: Analysis and visualization of channels and tunnels in protein structures and molecular dynamics trajectories. *Bioinform* **2018**, *34*, 3586–3588, doi:10.1093/bioinformatics/bty386.
33. Arduini, A.; Orlandini, G.; Secchi, A.; Credi, A.; Silvi, S.; Venturi, M. Calixarene Threading by Viologen Axles. In *Calixarenes and Beyond*, Neri, P.; Sessler, J.L.; Wang, M.-X., Eds.; Springer: Dordrecht, the Netherlands, **2016,** pp. 761–781, doi:10.1007/978-3-319-31867-7.
34. Schalley, C.A. *Analytical methods in supramolecular chemistry*, 2nd Edition; Wiley-VCH: Weinheim, Germany, 2012.

35. Suezawa, H.; Ishihara, S.; Umezawa, Y.; Tsuboyama, S.; Nishio, M. The aromatic CH/π hydrogen bond as an important factor in determining the relative stability of diastereomeric salts relevant to enantiomeric resolution—A crystallographic database study. *Eur. J. Org. Chem*. **2004**, 4816–4822, doi:10.1002/ejoc.200400373.
36. Weinhold, F.; Landis, C.R. *Valency and Bonding: A Natural Bond. Orbital Donor-Acceptor Perspective*, 1st ed.; Cambridge University Press: Cambridge, UK, 2005; doi:10.5860/choice.43-4035.
37. Johnson, E.R.; Keinan, S.; Mori-Sánchez, P.; Contreras-García, J.; Cohen, A.J.; Yang, W. Revealing noncovalent interactions. *J. Am. Chem. Soc.* **2010**, *132*, 6498–6506, doi:10.1021/ja100936w.
38. Talotta, C.; Concilio, G.; de Rosa, M.; Soriente, A.; Gaeta, C.; Rescifina, A.; Ballester, P.; Neri, P. Expanding coefficient: A parameter to assess the stability of induced-fit complexes. *Org. Lett.* **2021**, *23*, 1804–1808, doi:10.1021/acs.orglett.1c00165.
39. Vergura, S.; Scafato, P.; Belviso, S.; Superchi, S. Absolute configuration assignment from optical rotation data by means of biphenyl chiroptical probes. *Chem. Eur. J.* **2019**, *25*, 5682–5690, doi:10.1002/chem.201806435.
40. Giorgio, E.; Viglione, R.G.; Zanasi, R.; Rosini, C. Ab initio calculation of optical rotatory dispersion (ORD) curves: A simple and reliable approach to the assignment of the molecular absolute configuration. *J. Am. Chem. Soc.* **2004**, *126*, 12968–12976, doi:10.1021/ja046875l.